J Mater Sci (2006) 41:7096–7102
DOI 10.1007/s10853-006-0038-3

Crystallization process and electro-optical properties of In_2O_3 and ITO thin films

Frederick Ojo Adurodija · Lynne Semple · Ralf Brüning

Received: 20 May 2005 / Accepted: 23 September 2005 / Published online: 9 May 2006

Abstract Amorphous indium oxide (In_2O_3) and 10-wt% SnO_2 doped In_2O_3 (ITO) thin films were prepared by pulsed-laser deposition. These films were crystallized upon heating in vacuum at an effective heating rate of 0.00847 °C/s, while the evolution of the structure was observed by in situ X-ray diffraction measurements. Fast crystallization of the films is observed in the temperature ranges 165–210 °C and 185–230 °C for the In_2O_3 and ITO films, respectively. The crystallization kinetics is described by a reaction equation, with activation energies of 2.31 ± 0.06 eV and 2.41 eV and order of reactions of 0.75 ± 0.07 and 0.75 for the In_2O_3 and ITO films, respectively. The structures of the films observed here during heating are compared with those obtained upon film growth at different temperatures. The resistivity of the films depends on the evolution of the structure, the oxygen content and the activation of tin dopants in the films. A low resistivity of 5.5×10^{-4} Ω cm was obtained for the In_2O_3 and ITO films at room temperature, after annealing to 250 °C the resistivity of the ITO film reduces to 1.2×10^{-4} Ω cm.

Introduction

Indium oxide or indium-tin-oxide (In_2O_3 or ITO) film is a transparent conductor. It is found in many technological applications, including flat panel displays, solar energy and other optoelectronic devices because of its excellent combination of electrical and optical properties [1, 2]. In_2O_3 or ITO film exists in amorphous or crystalline phase. Crystalline films, which display better electro-optical properties, are acquired when the films are deposited on heated substrates or after annealing of the amorphous films. It has a complex cubic bixbyte Mn_2O_3 (I) structure emanating from a range of vacant tetrahedral oxygen anion sites. The structure of In_2O_3 film is affected by the growth conditions such as substrate temperature, oxygen pressure and deposition rate [1, 2].

The crystallization processes and dynamics of nucleation of In_2O_3 and ITO films have been reported [2–10]. The results show a disparity between the two materials and are sometimes dependent on the processing techniques. In the case of sputtering and pulsed laser deposition (PLD), the substrate temperature and the energy of the particles are found to have profound effect on the properties of the growing films [3]. During growths, the ratio of the amorphous to crystalline phase reduces with increasing temperature, the film still remaining partially amorphous at (150–165) °C, the so-called crystallization temperature [5, 11, 12]. Since the structures of the In_2O_3 and ITO films are directly related to their electrical and optical properties, a clear understanding of the crystallization kinetics is useful for applications where high-quality films have to be deposited at a low substrate temperature.

Studies of the crystallization of ITO or In_2O_3 films by X-ray diffraction (XRD) is commonly done on samples that have been cooled to room temperature after crystallization [4, 7, 9]. This method is uncertain because; (i) cooled samples may not represent the conditions at high temperature; (ii) the structure of the samples may alter on cooling; (iii) different samples are used which often makes reproduction of the sample conditions difficult. Indirect methods

F. O. Adurodija (✉) · L. Semple · R. Brüning
Department of Physics, Mount Allison University, E4L 1E6
Sackville, NB, Canada
e-mail: oadurodi@mta.ca

involving time dependent changes in the resistivity, reflectivity, or examination of the microstructure have been used to explain the crystallization of In_2O_3 and ITO films [5, 7]. These methods only presume that the change in the resistivity or reflectivity of the films during annealing translates into the amorphous–crystalline transition [5, 10]. Based on the different analytical techniques and differently prepared samples, crystallization temperatures ranging from 100 °C to 250 °C have been reported [3–10]. Thin film crystallization using real-time in situ XRD removes these doubts and has been rarely used for In_2O_3 or ITO films [3, 6].

We have followed the evolution of the structure of In_2O_3 and ITO by in situ XRD measurements at temperatures from 100 °C to 300 °C. The structures of the films observed here after heating are compared with those obtained upon film growth at different temperatures. The electrical and optical properties of the as-deposited films at different oxygen pressures and temperatures are also reported.

Experimental

In_2O_3 and ITO (In_2O_3 doped with 10 wt.% SnO_2) films were deposited using a Lambda Physik, COMPex 102 KrF (λ = 248 nm) excimer laser. Details on the PLD apparatus have been reported elsewhere [2]. Sintered ceramic In_2O_3 and ITO targets with a purity of 99.997% were used. The laser system was operated at an energy of ~230 mJ and a pulse frequency of 20 Hz. Amorphous and polycrystalline films were deposited on single crystal Si(100) substrates at oxygen pressures of 10^{-3} to 5×10^{-2} Torr and substrate temperatures of 23 °C (room temperature) to 300 °C. The nominal deposition rate and film thickness were 2 nm min^{-1} and 100 ± 20 nm, respectively.

The amorphous to crystalline transitions of the In_2O_3 and ITO film were monitored by XRD in vacuum during real-time annealing over temperatures ranging from 100 °C to 300 °C. The temperature was raised in steps of 5 °C at an effective heating rate of 0.00847 °C/s. The XRD analyses were performed using a Rigaku Rint-2000 and a custom built X-ray diffractometers with CuK_α radiation (λ = 1.542 Å). The custom built diffractometer operating in the θ–θ mode equipped with pyrolytic graphite monochromator and analyzer crystals, and a scintillation counter was used. The sample stage was mounted with a Boraelectric Heater capped with an aluminum plate. The sample was mounted on the aluminum plate with thermal paste to allow good thermal contact. The temperature difference between the heater and the sample was ±2 °C. To avoid air scattering, samples were measured in a vacuum chamber with a Kapton window at a pressure of 10^{-2} Torr. The scattered XRD intensity was measured as a function of the scattering angle, 2θ. Each measurement during the annealing is a composite of two 10 min interlaced scans. One set of points was measured while increasing 2θ from 28° to 32°, while a second set of points is obtained subsequently at decreasing 2θ values. The XRD peaks were fitted by Gaussian profile to obtain peak parameters such as the peak position, peak width, peak area and correction for resolution. The crystal sizes of the films were calculated from the peak parameters.

The resistivity of the annealed films was measured using a four-point probe. The thickness and the real part of the optical refractive index were determined by an ellipsometer (Mizojiri DVA-36L3), with He–Ne laser beam operating at a wavelength of 632.8 nm.

Results and discussion

Structural properties

Figure 1 shows the XRD spectra of the (222) peak for the In_2O_3 and ITO films annealed in situ at 100 °C to 300 °C. The diffraction patterns represent the real-time phase changes during the crystallization process. During the annealing of the amorphous films, In_2O_3 is found to crystallize at a lower temperature of 165 °C compared to ITO film at a temperature of 220 °C. The In_2O_3 film also displays stronger peak intensity. The 'zigzag' seen in the XRD spectra result from interlacing of the upward (28–32°) and downward (32–28°) 2θ XRD scans during the annealing cycle. Thus the unavoidable change of the sample state while measuring becomes apparent, rather than giving rise to an artificial shift of the peak in 2θ. Plots of the XRD peak intensity and crystal sizes versus annealing temperature are shown in Fig. 2. Below 165 °C, In_2O_3 film is amorphous as shown in Fig. 2a. The (222) peak appears at 165 °C, indicating the outset of crystallization. The intensity of the peak increases rapidly as the annealing temperature increases to 210 °C. A further increase in the annealing temperature produces no peak growth.

In contrast, a higher crystallization temperature of around 220 °C is observed for the ITO films as shown in Fig. 1b. At 230 °C a fully crystalline ITO film is attained. Because of the weak (222) reflection, evidence of crystallization could only be observed at around 220 °C in Fig. 2. But from the plots of the peak intensity versus annealing temperature in Fig. 2b, it appears that film crystallization starts at around 200 °C. The evolution of the (222) peak for In_2O_3 and ITO at annealing temperatures of (165–210 °C) and (200–230 °C), respectively, shows a rapid crystallization process, which is completed within 45 °C from the outset temperature. That is a total

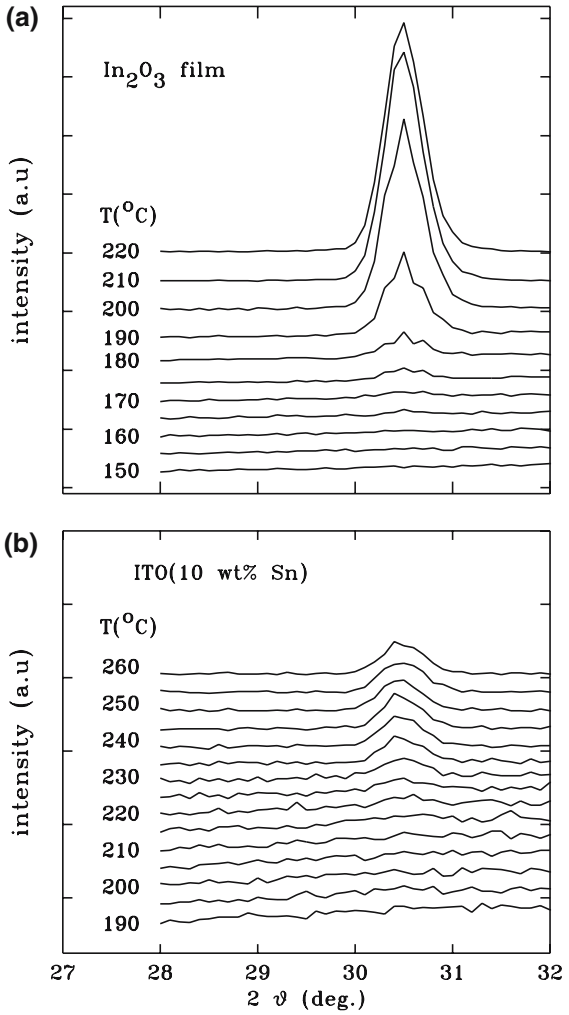

Fig. 1 XRD growth profile of (222) peak intensity for In_2O_3 and ITO films as a function of temperature, each measurement is interlace of two, 10 min scan

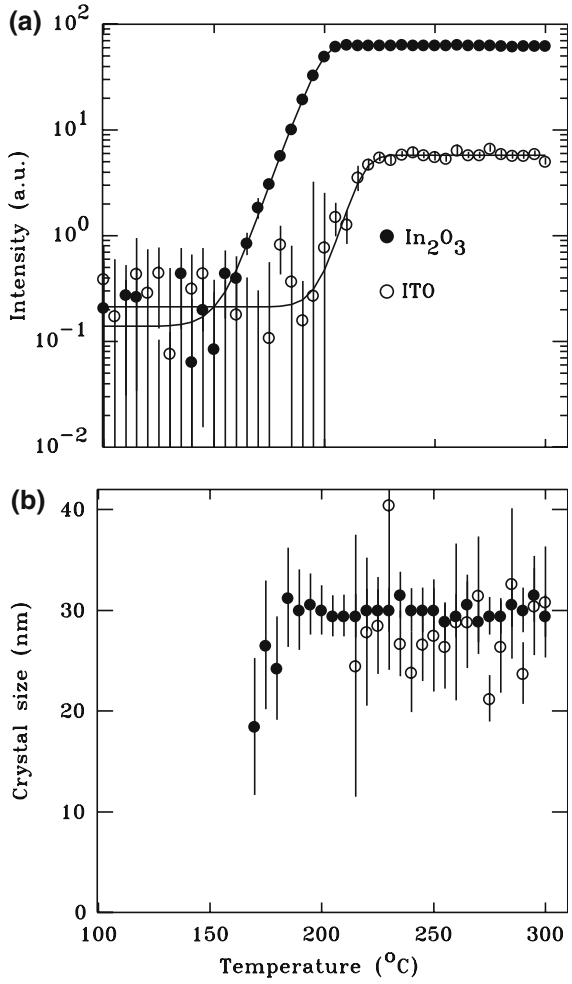

Fig. 2 (**a**) Growth of the integrated intensity of the In_2O_3 (222) and ITO peaks and (**b**) development of the crystal sizes of In_2O_3 and ITO films as a function of annealing temperature

time of 88 min for temperatures between 165 °C and 210 °C (including measuring times of 10 min per measurement under steady set temperatures). A transition in the crystallization mechanism is suspected to occur from pure grain nucleation to grain growth according to the structure zone model of thin films at temperatures of (165–210 °C) and (200–230 °C) for the In_2O_3 and ITO film, respectively [13]. A crystallization temperature of 165 °C agrees with that reported for In_2O_3 films [14–19]. However, different crystallization temperatures ranging from 150 °C to 250 °C have been reported for ITO films, including a recent work on real-time annealing of ITO films where a crystallization temperature of 250 °C was observed [6, 14–19]. Our findings are close to temperatures of 180 °C and 230 °C reported for sputter-annealed In_2O_3 and 10 wt. % SnO_2 doped In_2O_3 films, respectively [7]. The different crystallization temperatures may be due to the inclusion of Sn in the ITO crystal lattice.

Figure 2b shows the development of the crystal sizes as a function of the annealing temperature. The mean crystal sizes are obtained from the full width at half maximum of the (222) peak based on the Debye-Scherrer method [20]. The crystal sizes of the emerging crystallites could only be resolved at temperatures above 170 °C and 220 °C for the In_2O_3 and ITO films, respectively. For In_2O_3 film, the crystal size increases rapidly between 170 °C and 200 °C and then stabilizes with a further increase in the annealing temperature, suggesting growth and impingements of the crystallized regions of the film. For a fully crystallized film, average crystal sizes of 32 and 26 nm are obtained for the In_2O_3 and ITO films, respectively.

The crystallization kinetics is based on the following reaction rate equation:

$$\frac{\mathrm{d}N}{\mathrm{d}T} = \frac{A}{\varphi}(1 - N)^s \mathrm{e}^{\frac{-E}{kT}} \quad (1)$$

where E is the activation energy, and s is the order of reaction. T is temperature and A is frequency factor

The integral form of (1) gives.

$$N(T) = \frac{A}{\varphi}\int_0^T (1 - N)^s e^{\frac{-E}{kT}} dT \quad (2)$$

Fitting Eq. (2) to the growth profiles in Fig. 2a, produce activation energies of 2.31 ± 0.06 eV and 2.41 eV for In_2O_3 and ITO film, respectively. Reaction rate factor, $\log(A/\varphi)$, gives 21.7 ± 0.7 and 21.7 (fixed), while the order of reaction gives 0.75 ± 0.07 and 0.75 (fixed) for the In_2O_3 and ITO films, respectively. In_2O_3 film yields better estimates of the reaction parameters while fitting the reaction equation. The activation energies of the In_2O_3 and ITO materials are similar; however these values are higher than 0.67 ± 0.18 eV, 0.77 eV or 1.3 ± 0.2 eV reported in the literature [5, 8, 10]. The low reaction order of ~0.75 suggests that the crystallization kinetics is dominated by grain boundary nucleation/growth.

Figure 3 shows the full scan XRD spectra of the In_2O_3 and ITO films measured during annealing at 300 °C and at room temperature after the samples are cooled. The In_2O_3 films exhibit a strong (222) preferred orientation, but no preferred orientation is observed in the ITO films, Fig. 3a and b. The observation of peak at 33.1° (forbidden peak) belonging to Si(200) is due to the effect of the Si(100) substrate and it only occurs when the substrate is distorted [21]. The striking difference in the intensity of the Si(200) reflection contrasts the crystallilnity of In_2O_3 and ITO films. However, the suppression of the Si(200) peak intensity for the ITO sample (Fig. 3a) compared to Si(200) reflections for In_2O_3 sample (Fig. 3b) could originate from a mis-alignment of the Φ-axis which would move the scattered intensity originating from {k00} reflections of Si substrate out of coverage of the detector during the $\theta/2\theta$ scans. In general, better crystallinity is obtained in the In_2O_3 compared to ITO films. The calculated lattice constants for the In_2O_3 films at 300 °C and room temperature are 10.23 ± 0.20 Å and 10.14 ± 0.01 Å, respectively. For the ITO films, the lattice constant is 10.12 ± 0.01 Å at 300 °C and 10.16 ± 0.01 Å at room temperature. No major change in the lattice constant is observed between the heated and cooled samples and the values are close to the theoretical value of 10.12 Å for cubic In_2O_3.

Figure 4 shows the XRD spectra of In_2O_3 and ITO films deposited at different substrate temperatures at a fixed oxygen pressure of 10^{-2} Torr. The In_2O_3 film is amorphous below 150 °C. At 150 °C and above, polycrystalline cubic

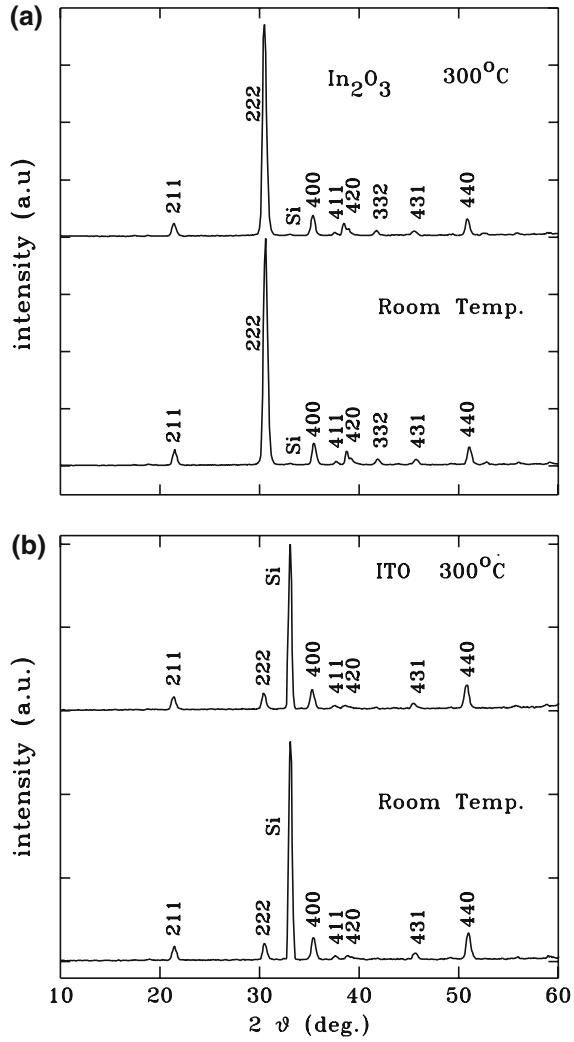

Fig. 3 XRD spectra of In_2O_3 and ITO films measured at 300 °C and after cooling to room temperature

bixbyite In_2O_3 appears. The film shows a preferred orientation along the (222) axis with increasing substrate temperature during the deposition. In the case of the ITO films, reflections are evident at room temperature. However, the (222) peak only appears at 200 °C and the film shows no preferential orientation.

In comparison, the crystallization temperature of In_2O_3 and ITO films deposited on heated substrates is lower than that of in situ annealed films, as shown in Figs. 1 and 4. It is known that energetic particle bombardment of the film surface during growths lowers the crystallization temperature [2, 6]. Therefore, the reduced crystallization temperature in the films deposited on heated substrate is caused by a rise of the chemical driving force due to energetic particles impinging on the film surface during growths [10, 14].

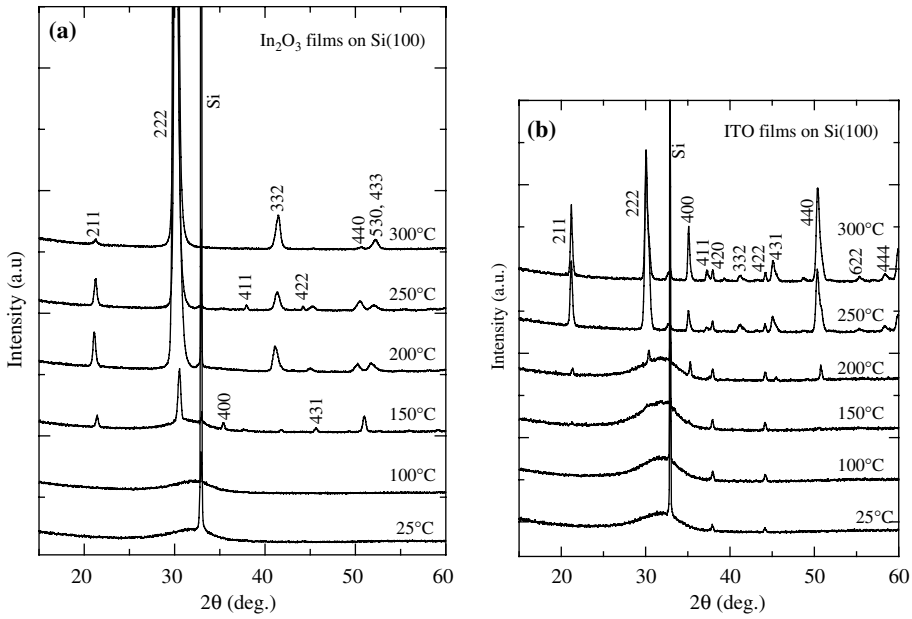

Fig. 4 XRD spectra of as-deposited (**a**) In_2O_3 and (**b**) ITO films on heated substrates at different temperatures

Electrical and optical properties

Figure 5 shows the dependence of the resistivity on the oxygen pressure for In_2O_3 and ITO films deposited at room temperature and 200 °C. At room temperature, comparable resistivities are achieved for the In_2O_3 and ITO films. However, the resistivity of the In_2O_3 film is slightly lower at 1×10^{-3} Torr. A minimum resistivity of 5.5×10^{-4} Ω cm is obtained for the In_2O_3 and ITO films at an oxygen pressure of 1×10^{-2} Torr. At higher oxygen pressures sharp increase in the resistivity of the films is noticed. For ITO films deposited at 200 °C, lower resistivities are obtained; however, the resistivity curves follow a similar trend with changes in the oxygen pressure. The resistivity of In_2O_3 is known to depend on the oxidation state of indium; hence the creation of oxygen vacancies dominated the free electron generation mechanism that lowered the resistivity of the In_2O_3 film [2, 16, 22–28].

Figure 6 shows the resistivity and the real part of the refractive index versus the substrate temperature for In_2O_3 and ITO films deposited at an oxygen pressure of 10^{-2} Torr. The resistivity of the films decreases with increasing substrate temperature up to around 150 °C (crystallization temperature) as shown in Fig. 6a. Above 150 °C, a marked rise in the resistivity of the In_2O_3 is noticed while that of ITO films continues to reduce exponentially with increasing substrate temperature. A minimum resistivity of 1.4×10^{-4} Ω cm is obtained for the ITO film above 250 °C. The sudden increase in the resistivity of the In_2O_3 films from 150 °C is associated with the depletion of oxygen vacancies upon crystallization [2, 7]. In ITO films, the presence of Sn lowers the resistivity due to thermal activation of Sn into Sn^{4+}: as Sn finds substitutional sites during crystallization, it adds extra free electrons to the conduction band [22, 25, 28]. In amorphous ITO film, Sn is not efficiently activated, hence the higher resistivity at lower substrate temperatures.

The real part of the refractive indices is shown in Fig. 6b. Due to limitations in our ellipsometry equipment, only the real part of the refractive index is measured, the imaginary part could not be provided. Moreover, since the samples were deposited on silicon substrates, other information such as transmittance, reflectance and absorption coefficients of the films could not be determined. Other researchers have used only the real-part of the refractive index to describe the optical properties of their ITO films [6, 29–31]. From Fig. 6b, it is observed that between room temperature and

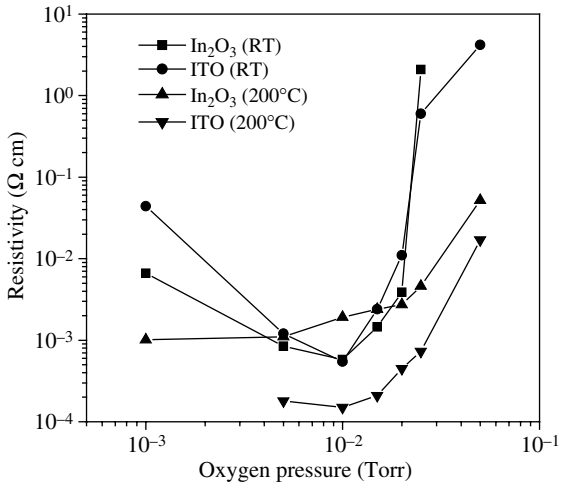

Fig. 5 Resistivity of In_2O_3 and ITO films deposited at different temperatures as a function of oxygen pressure

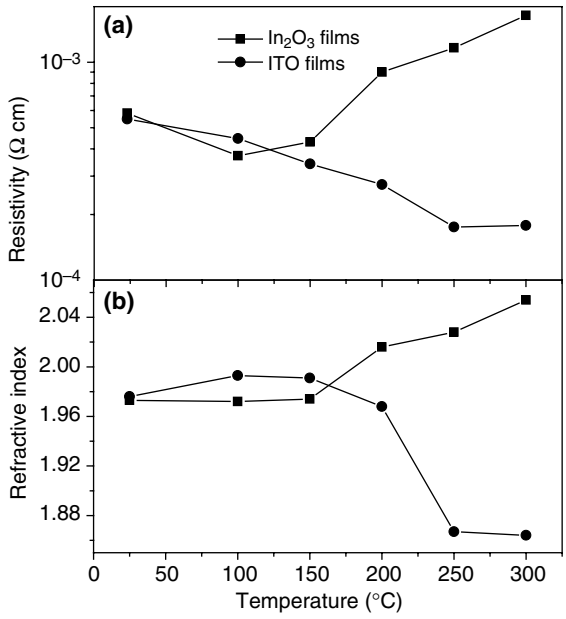

Fig. 6 (**a**) Resistivity and (**b**) Refractive indices of In_2O_3 and ITO films deposited at different temperatures and at an oxygen pressure of 1×10^{-2} Torr

150 °C, the refractive indices are comparable. Above 150 °C, the refractive index of the In_2O_3 films increases, while that of the ITO decreases rapidly with increasing substrate temperature. The crossover region of the two curves at around 165 °C coincides with the crystallization temperature of In_2O_3. The observed refractive indices of 1.87 to 2.24 fall within the limits reported for In_2O_3 and ITO films [6, 29–31]. Note that the behavior of the refractive index and the resistivity with deposition temperatures are closely related, indicating the deposition conditions and the presence of Sn in the films affect both the electrical and optical properties of the In_2O_3 and ITO films. It has been reported that a change in the refractive index with changes in the ratio of In_2O_3 and SnO_2 are associated with the carrier concentration of ITO films [32]. The changes in the refractive index can most reasonably be explained by the contribution of Sn or oxygen vacancies to the available carriers in the material, which affects the electro-optical properties of the films [33].

Conclusion

Amorphous indium oxide (In_2O_3) and 10-wt% SnO_2 doped In_2O_3 (ITO) thin films prepared by PLD were crystallized upon heating in vacuum at an effective heating rate of 0.00847 °C/s, while the evolution of the structure was observed by in situ XRD measurements. The films crystallized in the temperature ranges 165–210 °C and 200–230 °C for the In_2O_3 and ITO, respectively. The crystallization kinetics was described by activation energies of 2.31 ± 0.06 eV and 2.41 eV and reaction order of 0.75 ± 0.07 and 0.75 for the In_2O_3 and ITO films, respectively. The structures of the films observed here during heating were compared with those obtained upon film growth at different temperatures and the results show a lower crystallization temperature for films grown on heated substrates. The reduced crystallization temperature in the films deposited on heated substrates is ascribed to impinging energetic particles on the substrate surface during growths. The resistivity of the films depended on the evolution of the structure, the oxygen content and the activation of Sn dopants in the films. A low resistivity of 5×10^{-4} Ω cm was obtained for the In_2O_3 and ITO films at room temperature, while a value of 1.2×10^{-4} Ω cm was achieved for an ITO film at 250 °C.

Acknowledgments This project is partly sponsored by Atlantic Innovation Fund (AIF) and Natural Science and Engineering Research Council (NSERC).

References

1. Granqvist CG (2000) Solar Energy Mater Solar Cells 60:201
2. Adurodija FO (2001) In: Nalwa HS (ed) Handbook of thin films: deposition and processing of films, vol 1. Academic Press, New York, p 161
3. Ellmer K, Mientus R, Weiß V, Rossner H (2003) Meas Sci Technol 14:336
4. Diniz ASAC, Keily CJ (2004) Renewable Energy 29:2037
5. Ow-Yang CW, Springer D, Shigesato Y, Paine DC (1998) J Appl Phys 88:145
6. Rogozin A, Shevchenko N, Vinnichenko M, Prokert F, Cantelli V (2004) Appl Phys Lett 85:212
7. Morikawa H, Fujita M (2000) Thin Solid Films 359:61
8. Wulff H, Quaas M, Steffen H, Hippler R (2000) Thin Solid Films 377–378:418
9. Morikawa H, Sumi H, Kohyama M (1996) Thin Solid Films 281–282:202
10. Paine DC, Whitson T, Janiac D, Beresford R, Ow-Yang CW (1999) J Appl Phys 85:8445
11. Muranaka S, Bando Y, Tanaka T (1987) Thin Solid Films 25:35
12. Muranaka S (1991) Jpn J Appl Phys 30:L2062
13. De Beardemaeker J, Dauwe C, Deduytsche D, Detavernier C, Egger W, Sperr P (2004) Mater Sci Forum 445–446:69
14. Song PK, Shigesato Y, Yasui I, Ow-Yang CW, Paine DC (1998) Jpn J Appl Phys 37:1870
15. Oyama T, Hashimoto N, Shimazu J, Akao Y, Kojima H, Aikawa K, Suzuki K (1992) J Vac Sci Technol A 10:1682
16. Sun XW, Huang HC, Kwok HS (1996) Appl Phys Lett 68:2663
17. Thornton JA, Hoffman WD (1989) Thin Solid Films 171:5
18. Bardos L, Libra M (1989) Vacuum 39:33
19. Bender M, Katsarakis N, Gagaoudakis E, Hourdakis E, Douloufakis E, Cimalla V, Kiriakidis G (2001) J Appl Phys 90:5382
20. Bertaut E (1968) In: International tables for x-ray crystallography, vol 3. Kynoch Press, Birmingham, p 318
21. Zhao L, Steinhart M, Yosef M, Lee SK, Geppert T, Pippel E, Scholz R, Gosele U, Schecht S (2005) Chem Mater 17:3

22. Tahar RBH, Ban T, Ohya Y, Takahashi Y (1998) J Appl Phys 83:2631
23. Adurodija FO, Bruning R, Asia IO, H Izumi, Ishihara T, Yoshioka H (2005) Appl Phys A 81:953
24. Izumi H, Adurodija FO, Kaneyoshi H, Ishihara T, Yoshoika Y, Motoyama M (2002) J Appl Phys 91:1213
25. Kim H, Gilmore C, Pique A, Horwitz JS, Matoussi H, Murata H, Kafifi ZH, Chrisey DB (1999) J Appl Phys 86:6451
26. Kwok HS, Sun XW, Kim DH (1998) Thin Solid Films 335:229
27. Adurodija FO, Izumi H, Ishihara T, Yoshioka Y, Matsui H, Motoyama M (1999) Appl Phys Lett 74:3059
28. Yu Y, Maree CHM, Haglund RF Jr, Hamilton JD, Morales Paliza MA, Huang MB, Felman LC, Weller RA (1999) J Appl Phys 86:991
29. Jung YS (2004) Thin Solid Films 467:36
30. Martino M, Luches A, Fernandez M, Anobile P, Petruzzelli V (2001) J Phys D: Appl Phys 34:2606
31. Losurdo M, Griangregorio M, Capezzuto P, Bruno G, De Rosa R, Roca F, Summonte C, Pla J, Rizzoli R (2002) J Vac Sci Tech A 20:37
32. Chen RT, Robinson D (1992) Appl Phys Lett 60:1541
33. Yeom HY, Popovich N, Chason E, Paine DC (2002) Thin Solid Films 411:17